Jupiter's Whistler-mode Belts and Electron Slot Region

Y.-X. Hao[1,2], Y. Y. Shprits[1,3,4], J. D. Menietti[5], Z. Y. Liu[6], T. Averkamp[5], D. D. Wang[1], P. Kollmann[7], G. B. Hospodarsky[5], A. Drozdov[4], E. Roussos[2], N. Krupp[2], R. B. Horne[8], E. E. Woodfield[8] and S. J. Bolton[9]

Y.-X. Hao, GFZ German Research Centre for Geosciences, 14473 Potsdam, Germany; Now at Max Planck Institute for Solar System Research, 37077, Germany. (hao@mps.mpg.de)

[1]GFZ German Research Centre for Geosciences, 14473, Potsdam, Germany

[2]Max Planck Institute for Solar System Research, 37077, Goettingen, Germany

[3]Institute of Physics and Astrophysics, University of Potsdam, Germany

[4]University of California Los Angeles, Los Angeles, CA, USA

[5]Department of Physics and Astronomy, University of Iowa, Iowa City

The spatial distribution of whistler-mode wave emissions in the Jovian magnetosphere measured during the first 45 perijove orbits of Juno is investigated. A double-belt structure in whistler-mode wave intensity is revealed. Between the two whistler-mode belts, there exists a region devoid of 100s keV electrons near the magnetic equator at $9 < M < 16$. Insufficient source electron population in such an electron "slot" region is a possible explanation for the relatively lower wave activity compared to the whistler-mode belts. The wave intensity of the outer whistler-mode belt measured in the dusk-premidnight sector is significantly stronger than in the postmidnight-dawn sector. We suggest that the inherent dawn-dusk asymmetries in source electron distribution and/or auroral hiss emission rather than the modulation

[6]IRAP, CNRS-Universite Toulouse III Paul Sabatier, Toulouse, France

[7]Johns Hopkins University Applied Physics Laboratory, Laurel, MD, USA

[8]British Antarctic Survey, High Cross, Madingley Road, Cambridge, UK

[9]Space Science and Engineering Division, Southwest Research Institute, San Antonio, TX, USA

of solar cycle are more likely to result in the azimuthal variation of outer whistler-mode belt intensity during the first 45 Juno perijove orbits.

1. Introduction

As the magnetosphere with the most intense radiation belt(s) [e.g., *Mauk and Fox*, 2010] in our solar system, the Jovian magnetosphere is an attractive natural laboratory for studying wave-particle interactions. Plasma waves with frequency ranging from below the ion cyclotron frequency (e.g., Alfvén waves [*Saur et al.*, 2018]) to above the electron cyclotron frequency (e.g., Z-mode waves [*Menietti et al.*, 2023b]) contribute considerably to the dynamics of Jovian energetic electrons. Whistler-mode chorus and hiss waves, which have been demonstrated as key components to the terrestrial electron belt dynamics [*Horne et al.*, 2005; *Allison et al.*, 2021; *Li et al.*, 2015; *Zhao et al.*, 2019], are also key drivers of acceleration and loss of energetic electrons trapped in Jupiter's magnetic field [*Horne et al.*, 2008; *Shprits et al.*, 2012; *Woodfield et al.*, 2014].

Whistler-mode waves can drive both electron acceleration and loss. The quantification of their spatial and spectral distributions is necessary for evaluating their impact at Jupiter. A subset of measurements based on Galileo and Juno mission data [*Menietti et al.*, 2012, 2021a, b; *Li et al.*, 2020] have been analyzed. With the Juno Extended Mission updated to the 45th perijove orbits (PJ45) [e.g., *Menietti et al.*, 2023a], a larger section of the nightside Jovian magnetosphere within $25R_J$ (R_J denotes Jupiter radius) has been sampled, giving us the opportunity to build a more comprehensive global map of whistle-mode waves.

In this study, we focus on the spatial distribution of whistler-mode waves and their links to 30-800 keV electron spectra within $25R_J$, as measured by Juno during its first 45 perijove orbits. Unless otherwise stated, the wave frequency range is restricted to between $0.1f_{ceq}$ and $0.8f_{ceq}$ (f_{ceq} denotes the frequency of the equatorial electron cyclotron), whereas mapped energetic electron fluxes are selected within 4° of magnetic latitude. With the given frequency range we highlight the spatial distribution of whistler-mode chorus waves, even if the contribution of auroral hiss waves can not be fully excluded. Corresponding energetic electron measurements near the magnetic equator, where whistler-mode chorus waves are believed to be excited, are also analyzed for context.

2. Banded Chorus Waves Observed at the Magnetic Equator

Figure 1 shows an example of whistler-mode chorus emission measured by the Juno spacecraft near Jupiter's magnetic equator. The top/middle panel displays the electric/magnetic spectral density detected by the Juno Waves instrument [*Kurth et al.*, 2017] while the bottom panel shows their ratio E/cB. The harmonic structure above the local electron cyclotron frequency f_{ce} (calculated with local Juno magnetometer measurements [*Connerney et al.*, 2017]) was observed between ∼16:00-16:15, during a magnetic equator crossing. Large E/cB values indicate waves of an electrostatic nature. We note that such equatorial electrostatic waves with harmonic structure are tell-tale signatures of the electron cyclotron harmonics (ECH) emissions confined inside the plasma sheet of Jupiter [c.f., *Menietti et al.*, 2012, Figure 4].

In addition to ECH emissions above f_{ce}, emissions between $0.1f_{ce}$ and $0.8f_{ce}$ are also recorded in Figure 1. Calculated $E/cB < 1$ indicates a clear electromagnetic nature of these waves. At 15:45-15:55, the emission was confined between $0.1f_{ce}$ and $0.5f_{ce}$, is identified as typical lower band chorus waves. At 16:00-16:26, wave emissions were observed in both the $0.1f_{ce} - 0.5f_{ce}$ and $0.5f_{ce} - 1.0f_{ce}$ bands. Burst mode data of the Juno Waves instrument indicate that there existed a distinct power gap between the two frequency bands below and above $0.5f_{ce}$. Waves with such dual-band structure are reminiscent of whistler-mode chorus waves in the terrestrial magnetosphere [e.g., *Tsurutani and Smith*, 1974; *Teng et al.*, 2019].

3. Global Morphology of Whistler-mode Waves

Previous Juno-based studies [*Li et al.*, 2020; *Menietti et al.*, 2021a, b, 2023a] presented the spatial distribution of whistler-mode waves integrated power using f_{lh} or f_{ci} as the lower cutoff frequency (f_{lhr}: lower hybrid resonance, f_{ci} ion cyclotron frequency). We note that in these studies, wave intensities between the lower cutoff and $0.1f_{ce}$, which are likely to be (auroral) hiss waves, are much stronger than the wave intensities above $0.1f_{ce}$ ([e.g, *Li et al.*, 2020, Figure 4] and [*Menietti et al.*, 2021b, Figure 5]). Therefore, the global distributions of the integrated whistler-mode wave intensity in *Li et al.* [2020] and *Menietti et al.* [2021b] mostly depict the wave morphology below $0.1f_{ce}$. As discussed in Section 2, Juno measurements demonstrate two points that we adopt in the upcoming sections: 1. Whistler-mode chorus waves in the Jovian magnetosphere show a distinct frequency band structure similar to the terrestrial chorus waves [*Burtis and Helliwell*, 1969]; 2. The electron cyclotron frequency (f_{ceq}) could be a suitable normalization factor for the spectrum of Jovian chorus waves [*Menietti et al.*, 2021a, b], as done for terrestrial chorus waves [e.g., *Wang et al.*, 2019].

We focus on the spatial distribution of whistler-mode waves with the frequency range 0.1-0.8f_{ceq}, which is in the frequency range of “typical chorus waves” [e.g., *Tsurutani and Smith*, 1977; *Meredith et al.*, 2012; *Wang et al.*, 2019]. We follow the same methodology as for the whistler-mode survey as in *Menietti et al.* [2021a] with data up to PJ45 [*Menietti et al.*, 2023a]. The same spatial grid size is adopted ($\Delta M = 1.0$, $\Delta MLT = 1h$, $\Delta\lambda = 2°$ for $|\lambda| < 16°$ and $\lambda = 5°$ for $|\lambda| > 16°$, where M, MLT and λ denote the M shell, magnetic local time, and magnetic latitude, respectively) for spatial binning. The M-shell and f_{ceq} are based on the JRM09 plus current sheet model [*Connerney et al.*, 1981, 2018]. Spatial grids and the accumulative sampling time of Juno per bin are shown in supporting Figure S1. In this study, the outermost M-shell extends to 25, while the absolute value of magnetic latitude to 36°. Higher latitudes are excluded to minimize the influence of auroral hiss [e.g., Figure 4 of *Li et al.*, 2020]. In terms of MLT, the whole night sector of Jupiter is covered.

The integrated wave intensity $\langle B_W^2 \rangle$ in each step of spacecraft sampling (hereafter referred to as "data point") is the average value of the wave intensity measured over the time interval $\Delta\tau = 1\ min$. $\langle B_W^2 \rangle$ is calculated with

$$\langle B_W^2 \rangle = \langle \int_{uc}^{lc} PSD(f) df \rangle, \tag{1}$$

between $0.1 f_{ceq}$ and $0.8 f_{ceq}$ and $PSD(f)$ is the magnetic power spectral density. The frequency-resolved wave intensity $\langle B_{Wi}^2 \rangle$ is calculated within 7 normalized frequency ($\beta = f/f_{ceq}$) bins using:

$$\langle B_{Wi}^2 \rangle = \langle \int_{\beta_i - \frac{1}{2}\Delta\beta}^{\beta_i + \frac{1}{2}\Delta\beta} PSD(f_{ceq}\,\beta) f_{ceq}\, d\beta \rangle, \tag{2}$$

in which each bin centers from $\beta_0 = 0.15$ to $\beta_7 = 0.75$ with the bandwidth $\Delta\beta$=0.1.

Figure 2 presents the spatial distribution of the average integrated magnetic intensity for whisler-mode waves in the chorus frequency range. Surprisingly, the spatial distribution of whistler-mode wave intensity in typical chorus frequency range exhibits a double-belt structure. In addition to the intense whistler-mode emission at $5 < M < 9$, another "whistler-mode belt" emerges at $18 < M < 25$, peaking at $M \approx 21$. The outer whistler-mode belt is of the strongest intensity around dusk, indicating a possible dawn-dusk asymmetry of the wave emission. Panels (b) and (c) show the intensity of whistler-mode emission in the meridian plane, averaged over midnight to dawn and dusk to midnight, respectively. The outer whistler-mode belt is distinct in both sectors and extends at least up to $|\lambda| = 21°$. The outer belt whistler-mode wave intensity at the dusk-midnight sector is stronger in each corresponding $(M, |\lambda|)$ bin, suggesting that the observed dawn-dusk asymmetry is not due to an orbital bias.

3.1. Double-Belt Structure of Whistler-mode Wave Intensity

In Figure 3 we present the median, upper, and lower quartile of whistler-mode wave intensity as a function of M-shell. Since intense whistler-mode wave emissions have been reported during Ganymede and Europa flybys [*Gurnett et al.*, 1996; *Shprits et al.*, 2018; *Kurth et al.*, 2022], possible Galilean-moon flybys have been excluded from our analysis.

As shown in Figure 3(a), the median wave intensity of whistler-mode wave exhibits a distinct double-peaked distribution along the M-shell. The median value of integrated wave intensity at the belt peaks is comparable ($2 \times 10^{-5} nT^2 \sim 3 \times 10^{-5} nT^2$). The "slot region" in between the two belts lies roughly between $M = 9$ and 16 with an intensity minimum of one order of magnitude lower than at the peaks, located at $M \approx 11$. We further note that within the entire M-shell range, the highest contribution ot the integrated intensity comes for the $0.1f_{ceq} - 0.2f_{ceq}$ range. This statistical wave frequency spectrum is consistent with previous studies [c.f., Figure 5(b) of *Menietti et al.*, 2021b].

To explore the possible mechanisms behind the dual whistler belt structure, we investigate the distribution of energetic electrons measured by Jupiter Energetic-particle Detector Instrument (Juno/JEDI)[*Mauk et al.*, 2017], using publicly available data up to PJ44. As various studies [e.g., *Burton and Holzer*, 1974; *Tsurutani and Smith*, 1977; *Lauben et al.*, 2002] have shown, whistler-mode chorus waves at Earth are excited near the magnetic equator, therefore we focus on electrons populations measured within 4° of magnetic latitude. JEDI measurements during time intervals with "high resolution" spectra have been interpolated into the "low resolution" energy bins, assuming local power-law spectra between adjacent energy channels. Figure 3(b) presents the median-averaged distribution of omni-directional differential fluxes for 30-800 keV electrons within M=25.

We note that there exists a slot-like region of energetic electrons between 9<M<16, where a flux depletion of 100s keV electrons by over 2 orders of magnitude is identified. Such energy-dependent depletion was also seen partially in previous studies [e.g., *Wang et al.*, 2021, Figure 4]. In Figure S2, we present both the median and mean values of the electron fluxes as a function of the M-shell measured during the first 29 (interval studied by [*Ma et al.*, 2021]) and 44 orbits (this study) of Juno. We note that due to the ascending perijove latitude of Juno, orbits PJ01-PJ29 did not cover the near-equator region at $M < 9$ and conclude that the slot's appearance is not an averaging method or data sampling artefact. Most notable, the energetic electron slot coincides with the one of Jovian whistler-mode waves.

We calculate the characteristic energy E_C and total energy flux ϵ_T of the energetic electrons [*Mauk et al.*, 2004]. As shown in Figure 3(c), characteristic energy of the electron energy spectra drops steeply down to $\sim 40keV$ at $M \approx 9$ and recovers to $\sim 100keV$ at $M \approx 16$, indicating much softer electron spectra inside the whistler-mode slot region than in the whistler-mode belts.

The total energy flux ϵ_T of energetic electrons with differential flux j(E) is calculated with

$$\epsilon_T = 4\pi \int_{E_{min}}^{E_{max}} j \cdot E \; dE. \tag{3}$$

The factor 4π is used for the omni-directional electron population measured near the magnetic equator. The dark blue curve and error bars in Figure 3(c) show the median value, lower and upper quartile of T as a function of M-shell. Sharp decreases in T are distinct at $M \approx 9$ and $M \approx 16$, the boundaries of electron slot region.

The colocation of the Jovian whistler-mode and energetic electrons slot regions is likely not a coincidence. Previous studies [*Menietti et al.*, 2021a, b] suggest that whistler-mode dynamics in Jovian inner and middle magnetosphere are controlled by the intensity of 100s keV electrons. The cyclotron resonance condition between electrons and whistler-mode waves can be expressed as

$$\omega - k_{\parallel} v_{\parallel} = n|\Omega_e|/\gamma, \tag{4}$$

where $k_{\parallel}$ and $v_{\parallel}$ are the field-aligned components of the wave propagation vector and particle velocity, ω and $\Omega_e = 2\pi f_{ce}$ are the angular frequency of the wave and electrons,

γ is the relativistic factor and $n = 0, \pm 1, \pm 2, ...$ is an integer referred to as the order of cyclotron resonance.

Equation 4 is used to calculate the minimum resonant energy (MRE) for the first-order cyclotron resonance ($n = 1$) between electrons and whistler-mode waves, which mainly control the growth and damping rates of whistler-mode chorus waves along with the Landau resonance ($n = 0$) [*Kennel and Petschek*, 1966; *Li et al.*, 2010]. A plasma density model from Galileo measurements [*Frank et al.*, 2002] is used. The red curves in Figure 3(c) show the MRE for electrons in the $n = 1$ cyclotron resonance with the $f = 0.1f_{ce}$ and $f = 0.5f_{ce}$ field-aligned whistler-mode waves, respectively. Our calculation shows that for the $n = 1$ MRE for electrons and whistler-mode waves in the equatorial lower band chorus frequency range at the magnetic equator (the chorus source region) occurs in the 10s to 100s of keV range at $5 \sim 25R_J$. Such a minimum resonance energy is close to the estimated characteristic electron energy.

Panels (d) and (e) of Figure 3 present the statistical pitch angle distribution (PAD) of electrons with an energy of ∼178.6 keV and ∼334.0 keV, respectively. Color-coded maps show the median value of the pitch angle-resolved differential electron fluxes in each (M, α) grid ($\Delta M = 0.5$, $\Delta\alpha = 10°$), where α denotes the local pitch angle. We note that above $M = 21$, where the outer whistler-mode belt peaks, the bidirectional PAD distributions dominate, in agreement with Galileo observations [*Tomás et al.*, 2004; *Mauk and Saur*, 2007] that a correlation between the PAD transition and the mapping of Jovian diffuse auroral emissions was indicated. Leakage of auroral hiss waves from the diffuse auroral zone may also contribute to the whistler-mode wave intensity in our statistics (detailed in

Section 3.2). *Saur et al.* [2018] developed a theory of wave-particle interactions between kinetic Alfvén waves (KAWs) and electrons in the Jovian magnetosphere, suggesting that KAWs are capable of generating broadband bidirectional auroral electron beams. Further investigation of the relationship among whistler-mode waves, bidirectional electron beams, and KAWs is needed to reveal the mechanism of the outer-belt whistler-mode excitation and the Jovian diffuse-aurora emission.

3.2. Local-time and Latitudinal Distribution of the Outer Whistler-mode Belt

As shown in Figure 2, the Juno extended mission reveals a stronger outer whistler-mode belt measured in the dusk-premidnight sector than in the postmidnight-dawn sector. As it took more than 6 years for Juno to scan from MLT0600 to MLT1800, such a variation of wave intensity could either result from a temporal variation or a spatial asymmetry. In this section, both scenarios will be examined.

The top panel of the supporting information Figure S3 presents the solar wind speed and Lyman-alpha intensity during the time interval of the Juno orbit PJ01-PJ45. For the first 45 orbits around Jupiter, Juno experienced both the descending phase of Solar Cycle 24 and the ascending phase of Solar Cycle 25. More high-speed solar wind events were recorded during the descending phase of Solar Cycle 24 than during the ascending phase of Solar Cycle 25. In contrast, the integrated chorus wave power measured in the outer whistler-mode belt ($18 < M < 25$) increased almost monotonically from $6 \times 10^{-6} nT^2$ to $7 \times 10^{-6} nT^2$ (see the bottom panel of Figure S3). Therefore, the long-term intensity variation of the outer whistler-mode belt is not positively correlated with the solar cycles.

The observed intensity variation is more likely to be an inherent dawn-dusk asymmetry in the Jovian magnetosphere.

Figure 4 presents the intensity of the outer whistler-mode belt and the energetic electron flux as a function of MLT. As the apogee of Juno precessed from the dawn to dusk, both the integrated whistler-mode wave intensity and the energetic electron flux increased nearly monotonically. Dusk intensities are around seven times stronger than at dawn. A similar asymmetry trend is seen in energetic electrons (panel b). The energy spectrum measured at dusk is also harder than at dawn. Since near-equatorial of 10s-100s keV electrons are potential sources of outer-belt whistler-mode emissions (Section 3.1), we suggest that such dawn-dusk asymmetries in both waves and energetic electrons spectra are likely interconnected.

It is worth noting that in the analysis above the contribution of auroral hiss waves cannot be fully eliminated [e.g., *Li et al.*, 2020; *Menietti et al.*, 2021b, 2023a]. Auroral hiss has a source region in the auroral region and is observed by Juno at higher magnetic latitudes and M-shells, and can be observed for large distances from its origin [*Gurnett et al.*, 1983; *Sazhin et al.*, 1993]. *Menietti et al.* [2023a] set a limit on observations of Jovian chorus emission at $|\lambda| < 31°$ or $M < 20$. At a larger M-shell or higher magnetic latitude, auroral hiss waves could become the dominant source of whistler-mode emission. In Figure S4, we show an example of intense whistler-mode auroral hiss emission. This is distinguished by the spectrogram wave morphology in the top two panels of Figure S4, showing a generally smooth appearance with no distinct narrow band signature as in the case of chorus. Chorus is known to have a source near the magnetic equator [cf.

Hospodarsky et al., 2012]. The waves shown in Figure S4 propagate away from Jupiter and toward the magnetic equator, which is consistent with auroral hiss. This is shown by analyzing the phase of the waves relative to the E_y and B_z antennas of the Juno Waves plasma wave instrument, as described in *Kolmašová et al.* [2018].

Distinguishing auroral hiss waves from chorus waves with the method shown above requires burst-mode Juno Waves data, which are not always available for our study. Here we attempt to identify the contribution of chorus and auroral hiss from the latitudinal distribution of the wave intensity, shown Figure 2(b-c). For the inner whistler-mode belt ($M < 12$), strong whistler-mode emissions concentrate in the near-equatorial region. Therefore, the inner whistler-mode belt is more likely to be dominated by chorus waves. For the outer-whistler belt, in the midnight-dawn sector there is also a peak of near-equatorial wave intensity ($|\lambda| < 8°$), indicating a possible contribution of chorus waves generated near the magnetic equator. In the dusk-midnight sector, the latitudinal dependence in mean wave intensity is not clear. In Figure 4(c), we further present the median value of wave intensity in the outer whistler-mode belt. In midnight-dawn sector, the median value also shows a peak within $|\lambda| < 16°$, which is most likely to be near-equatorial chorus waves rather than auroral hiss waves. At $|\lambda| \approx 23.5°$, another peak of the median wave intensity appears, indicating the contribution of auroral hiss waves. In the dusk-premidnight sector, the median wave intensity increases with $|\lambda|$ in the region $0° \leq |\lambda| < 16°$ and drops dramatically at $|\lambda| \approx 18.5°$. We note that for the $|\lambda| > 16°$ region, the orbital coverage of Juno was limited in the dusk-midnight sector. Therefore, it is hard to derive a complete latitudinal dependence of the wave intensity in the dusk-midnight sector from the Juno measurements. Based on our analysis above, we suggest that the "outer whistler-mode belt" may consist of equatorial chorus waves and auroral hiss waves from the Jovian polar region. Orbit-by-orbit analysis of wave properties is needed to further reveal the physical nature of the intense wave emission at $18 < M < 25$.

4. Summary and Discussion

Using by the Juno spacecraft during its primary and extended mission, we resolve several concurrent features in whistler wave and energetic electron intensities:

1. There is a double-belt structure in the intensity of Jovian whistler-mode waves ($0.1f_{ceq} < f < 0.8f_{ceq}$) between M=5 and 25. An outer whistler-mode belt peaks at $M \approx 21$ and shows wave intensity comparable to an inner whistler-mode belt at $M < 9$.

2. Between the aforementioned whistler-mode belts, a "slot" region of low energetic electron fluxes is revealed. At the region where $9 < M < 16$ and $|\lambda| < 4°$, the median fluxes of 100-700 keV electrons drop by over 2 orders of magnitude compared to the ambient environment. At $M \approx 21$, where the outer whistler-mode belt peaks, the pancake pitch angle distribution of 100 keV electrons switches to a bidirectional distribution.

3. The intensity of waves observed in the dusk-midnight sector of the outer whistler-mode belt is significantly higher than in the midnight-dawn sector. Fluxes of energetic electrons show a similar trend. Such distributions are most likely due to an inherent dawn-dusk asymmetry of the Jovian magnetosphere.

4. According to the latitudinal dependence of the wave intensity, the outer whistler-mode belt is a mixture of near-equatorial chorus waves and auroral hiss.

Since this study focused on the frequency range above $0.1 f_{ceq}$, it is no surprise that the spatial distribution patterns of wave intensity differ from previous studies starting from the local proton frequency (f_{cp}) or the lower hybrid frequency (f_{lh}), with which waves of lower frequency are counted [*Li et al.*, 2020; *Menietti et al.*, 2021a, b].

Juno observations have shown that the global distribution patterns of whistler-mode waves and 100s of keV electrons share mutual features in both the radial and azimuthal dimensions. Estimation of the minimum resonant energy for the $n = 1$ cyclotron resonance indicates that the aforementioned electron population is likely to be the source electrons that excite the whistler-mode waves. Given that such a peculiar global distribution pattern of waves could be fully explained by the observed electron distribution pattern, the mechanism that forms such an electron distribution map still remains enigmatic. Some possible explanations are briefly discussed below.

Radial diffusion process alone cannot account for the presence of the electron slot. Losses (absorption, scattering), and/or local acceleration are needed. Wave-particle interactions at higher latitude (e.g., inside the auroral zone [*Saur et al.*, 2018; *Elliott et al.*, 2018]) or from different frequency ranges than studied here (e.g., higher frequence Z-mode waves [*Menietti et al.*, 2021b] or lower frequency EMIC/hiss waves [*Li et al.*, 2020]) may be responsible. Comprehensive Fokker-Planck simulations considering realistic wave species and distribution [e.g., *Nénon et al.*, 2017] may help to understand the role of wave-particle interactions in the formation of the electron slot found in this study. We also highlight that the inner and outer edges of the electron slot are located at $M \approx 9$ and $M \approx 16$, which coincide with the orbits of Europa and Ganymede. Both satellites produce intense whistler-mode wave emissions [*Shprits et al.*, 2018; *Kurth et al.*, 2022]. These localized but very strong wave sources can drive local electron acceleration or loss [*Shprits et al.*, 2018; *Li et al.*, 2023].

Regarding the dawn-dusk electron flux asymmetry, several sources may account for them [*Palmaerts et al.*, 2017, and references therein]. The brightness of the Io torus has a significant dawn-dusk asymmetry [*Schneider and Trauger*, 1995; *Murakami et al.*, 2016], which is believed to be driven by the dawn-to-dusk electric field [*Barbosa and Kivelson*, 1983; *Ip and Goertz*, 1983]. Such a dawn-to-dusk electric field has also recently been utilized to explain the prompt acceleration of multi-MeV electrons at $M > 14R_J$ [*Roussos et al.*, 2018; *Hao et al.*, 2020; *Yuan et al.*, 2021]. We suggest that the dawn-to-dusk electric field may also explain the higher flux and harder energy spectra observed by both Juno/JEDI (this study) and Galileo/EPD [*Yuan et al.*, 2024] at dusk in comparison to the dawn flank. Another possible mechanism could be related to the corotation breakdown. Previous studies on ion flow anisotropies [*Krupp et al.*, 2001; *Waldrop et al.*, 2015] indicated that the corotation of the Jovian plasma starts to breakdown at $15 \sim 20R_J$ in the dusk sector while remaining rigid or even super-corotational in the dawn sector. Corotation breakdown may supply the heating and increase in the anisotropy of energetic electrons and hence lead to stronger chorus wave emissions in the dusk magnetosphere. Theoretical studies [*Kivelson and Southwood*, 2005; *Vogt et al.*, 2014] also discussed how centrifugal forces contribute to particle anisotropy and their local time asymmetry during outward expansion of flux tubes, which might also be related to dawn-dusk asymmetries in energetic electron distributions reported in this study.

Finally, the possibility that long-term temporal variations resulted in the observed inhomogeneity of the outer whistler-mode belt cannot be completely ruled out, as it took 6.1 years for Juno to achieve the map shown in Figure 2(a), approximately half of the orbital period of Jupiter (11.86 years). Although in Section 3.2 we have shown that the intensity of the outer whistler-mode belt is not likely to be positively correlated with solar activity, the seasonal effect remains a potential explanation for the observed variations in the Juno data. The strength of the coupling between the solar activity and the inner magnetosphere of Jupiter remains an open question. Furthermore, due to the lack of Juno equatorial coverage at MLT0000-0600 and $M < 12$, only the asymmetry of the outer whistler-mode belt is discussed in the present study. Combining Galileo data [e.g., *Menietti et al.*, 2012; *Shprits et al.*, 2018; *Li et al.*, 2020] with Juno data may help to draw a more conclusive picture of the whistler-mode wave distribution and temporal variation after undergoing the necessary cross-calibrations.

5. Acknowledgement

Y. Y. S, J. D. M and T. F. A are supported by the NASA Survey of Jovian Plasma Wave Intensity and Diffusive Modeling of Electron Acceleration and Scattering of Juno Participating Scientist Program (80NSSC19K1262). Y. Y. S declares potential conflict of interest and significant financial interest in Space Sciences Innovations Inc. in Seattle, WA. The authors sincerely acknowledge Margaret G. Kivelson and Xianzhe Jia for the discussion section.

6. Data Availablity Statement

Juno JEDI data can be obtained at https://pds-ppi.igpp.ucla.edu/search/view/?f=yes&id=pds://PPI/JNO-J-JED-3-CDR-V1.0. Juno WAV data can be obtained at https://pds-ppi.igpp.ucla.edu/search/view/?f=yes&id=pds://PPI/JNO-E_J_SS-WAV-3-CDR-SRVFULL-V2.0. Solar wind speed data can be obtained at https://cdaweb.gsfc.nasa.gov/sp_phys/data/omni/hro_1min/. Solar Lyman-alpha intensity data can be obtained at https://cdaweb.gsfc.nasa.gov/sp_phys/data/omni/hro_1min/

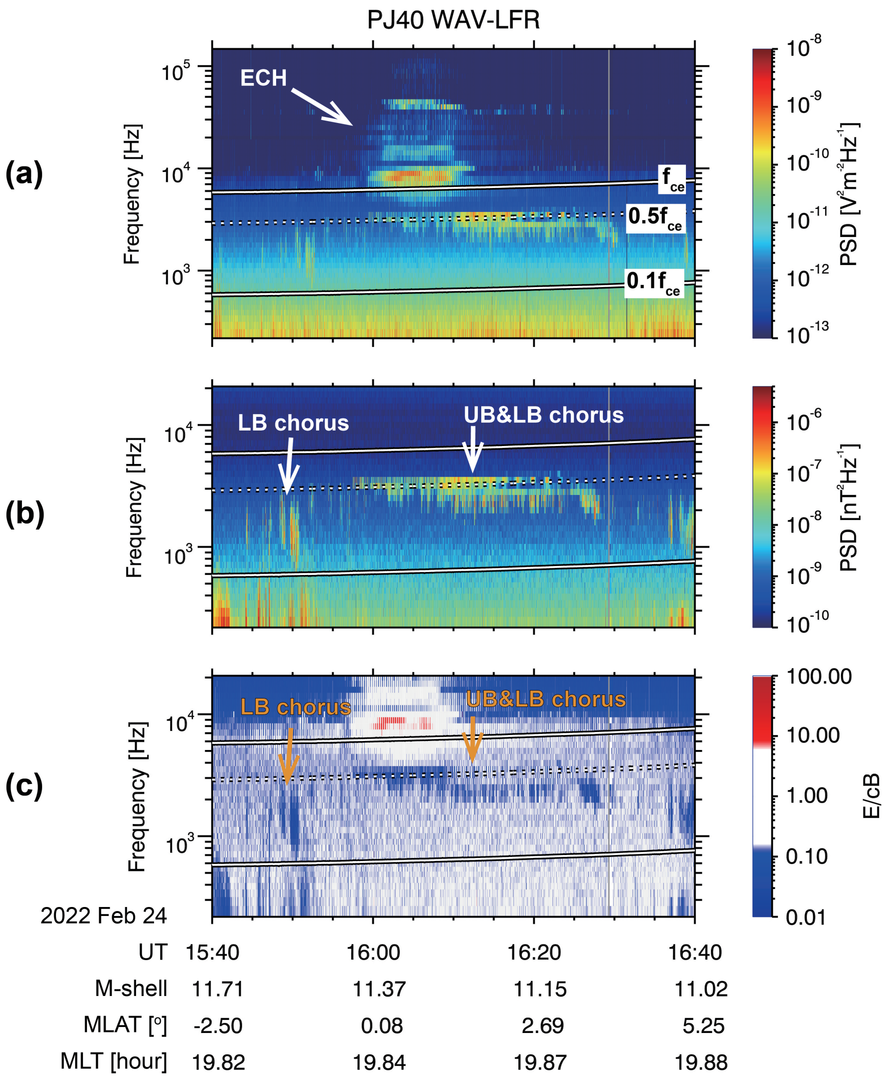

Figure 1. An example of whistler mode chorus waves observed by Juno near the magnetic equator of Jupiter. **(a)** Wave electrical power spectral density (PSD), **(b)** Wave magnetic PDSD, **(c)** E/cB during a magnetic equator passage of Juno's PJ40 orbit, showing ECH waves, lower-band (LB) and upper-band (UB) chorus. White curves in each panel indicate local f_{ce}, $0.5f_{ce}$ and $0.1f_{ce}$ values.

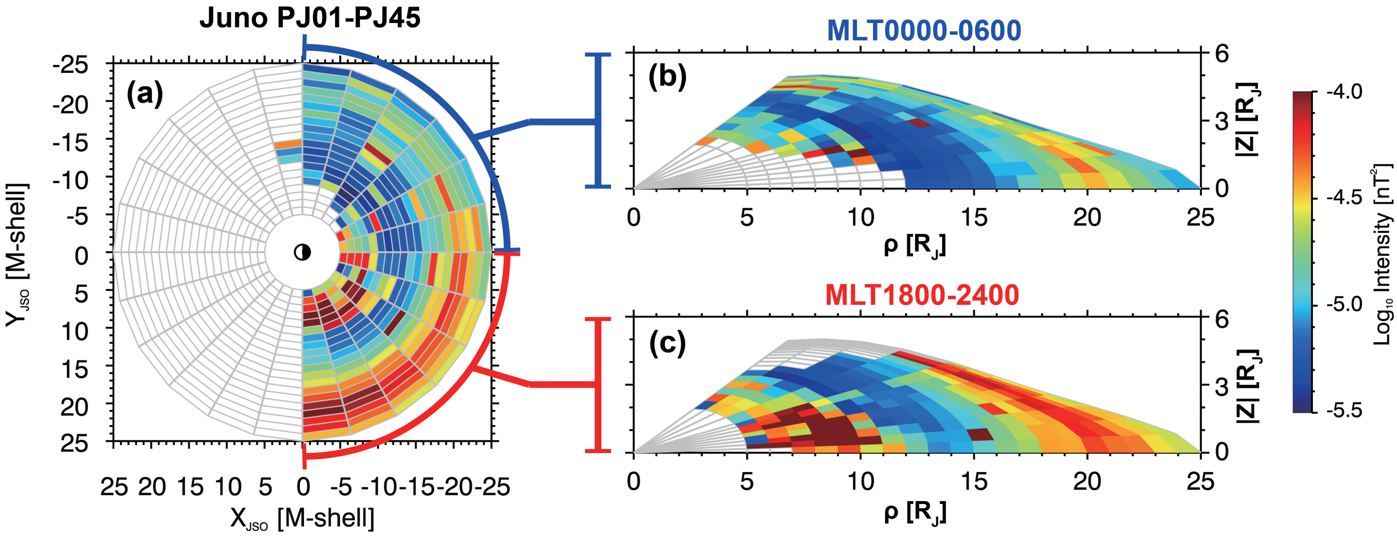

Figure 2. Whistler-mode wave intensity distribution. **(a)** M-shell versus MLT intensity spectrogram. **(b, c)** Wave intensity spectrogram in meridian plane for two MLT ranges. **(c)** Same format as panel (b) but for MLT from 1800 to 2400 (dusk-premidnight sector). Color coded are mean values of integrated wave intensity $\langle B_W^2 \rangle$ integrated between $0.1 f_{ceq} < f < 0.8 f_{ceq}$.

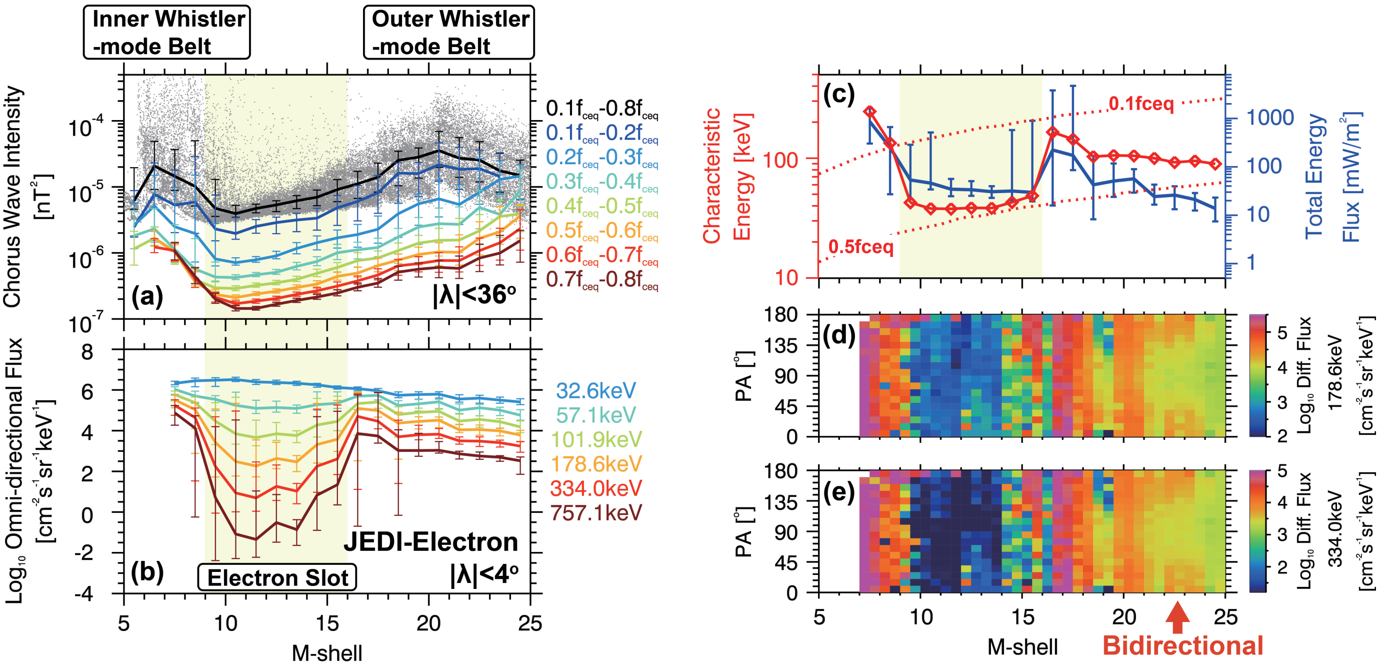

Figure 3. Statistical radial profile of whistler-mode waves and energetic electrons measured by Juno during orbits PJ01 through PJ45. **(a)** Whistler-mode wave intensity against M-shell. The gray points are 1-minute averaged wave intensities. Solid curves present median values of wave intensity in each frequency bin (colored) and total integrated wave intensity (black). **(b)** Median omni-directional electron differential fluxes against M-shell measured near the magnetic equator. **(c)** Characteristic energy and total energy flux derived from JEDI measurements. Dotted curves show the minimum energy for cyclotron resonance between electrons and whistler-mode waves with the frequencies $0.1f_{ceq}$ and $0.5f_{ceq}$. The energetic electron slot is marked with light yellow. **(d)-(e)** Median pitch angle distribution of ~179keV and ~334keV electrons.

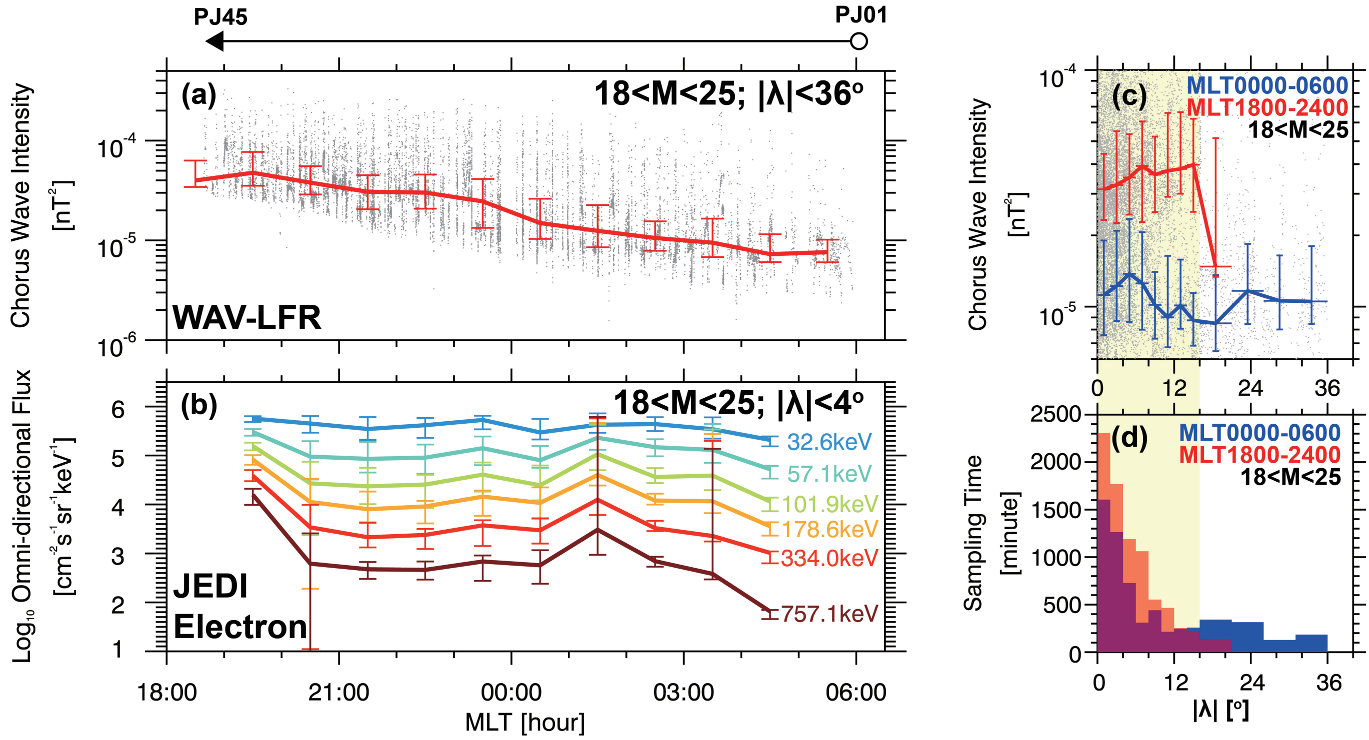

Figure 4. Local time asymmetry of the wave intensity and electron flux in the outer whistler-mode belt. **(a)** Whistler-mode wave intensity as a function of MLT. The solid curve shows the median wave intensity integrated from $0.1f_{ceq}$ to $0.8f_{ceq}$ within $18 < M < 25$ and $|\lambda| < 36°$. Gray points show the scatter plot of 1-minute averaged, wave intensity integrated from $0.1f_{ceq}$ to $0.8f_{ceq}$. **(b)** Median, upper, and lower quartiles of omnidirectional electron fluxes as a function of the MLT measured near the magnetic equator. **(c)** Integrated wave intensity as a function of $|\lambda|$. Blue (red) curve denotes the median wave intensity sampled in the midnight-dawn (dusk-midnight) sector. Gray points are the same data as in panel (a) but plotted as against $|\lambda|$. **(d)** Sampling time as a function of $|\lambda|$ at $18 < M < 25$ in each MLT sector.

References

Allison, H. J., Y. Y. Shprits, I. S. Zhelavskaya, D. Wang, and A. G. Smirnov, Gyroresonant wave-particle interactions with chorus waves during extreme depletions of plasma density in the van allen radiation belts, *Science Advances*, *7*(5), eabc0380, 2021.

Barbosa, D., and M. Kivelson, Dawn-dusk electric field asymmetry of the io plasma torus, *Geophysical Research Letters*, *10*(3), 210–213, 1983.

Burtis, W., and R. Helliwell, Banded chorus—a new type of vlf radiation observed in the magnetosphere by ogo 1 and ogo 3, *Journal of Geophysical Research*, *74*(11), 3002–3010, 1969.

Burton, R. K., and R. E. Holzer, The origin and propagation of chorus in the outer magnetosphere, *Journal of Geophysical Research*, *79*(7), 1014–1023, 1974.

Connerney, J., M. Acuna, and N. Ness, Modeling the jovian current sheet and inner magnetosphere, *Journal of Geophysical Research: Space Physics*, *86*(A10), 8370–8384, 1981.

Connerney, J., et al., The juno magnetic field investigation, *Space Science Reviews*, *213*, 39–138, 2017.

Connerney, J., et al., A new model of jupiter's magnetic field from juno's first nine orbits, *Geophysical Research Letters*, *45*(6), 2590–2596, 2018.

Elliott, S., D. Gurnett, W. Kurth, B. Mauk, R. Ebert, G. Clark, P. Valek, F. Allegrini, and S. Bolton, The acceleration of electrons to high energies over the jovian polar cap via whistler mode wave-particle interactions, *Journal of Geophysical Research: Space Physics*, *123*(9), 7523–7533, 2018.

Frank, L., W. Paterson, and K. Khurana, Observations of thermal plasmas in jupiter's magnetotail, *Journal of Geophysical Research: Space Physics*, *107*(A1), SIA–1, 2002.

Gurnett, D., W. Kurth, A. Roux, S. Bolton, and C. Kennel, Evidence for a magnetosphere at ganymede from plasma-wave observations by the galileo spacecraft, *Nature*, *384*(6609), 535–537, 1996.

Gurnett, D. A., S. D. Shawhan, and R. R. Shaw, Auroral hiss, z mode radiation, and auroral kilometric radiation in the polar magnetosphere: De 1 observations, *Journal of Geophysical Research: Space Physics*, *88*(A1), 329–340, 1983.

Hao, Y.-X., et al., The formation of saturn's and jupiter's electron radiation belts by magnetospheric electric fields, *The Astrophysical Journal Letters*, *905*(1), L10, 2020.

Horne, R. B., R. M. Thorne, S. A. Glauert, J. Douglas Menietti, Y. Y. Shprits, and D. A. Gurnett, Gyro-resonant electron acceleration at jupiter, *Nature Physics*, *4*(4), 301–304, 2008.

Horne, R. B., et al., Wave acceleration of electrons in the van allen radiation belts, *Nature*, *437*(7056), 227–230, 2005.

Hospodarsky, G., K. Sigsbee, J. Leisner, J. Menietti, W. Kurth, D. Gurnett, C. Kletzing, and O. Santolík, Plasma wave observations at earth, jupiter, and saturn, *Dynamics of the Earth's radiation belts and inner magnetosphere*, *199*, 415–430, 2012.

Ip, W.-H., and C. Goertz, An interpretation of the dawn–dusk asymmetry of uv emission from the io plasma torus, *Nature*, *302*(5905), 232–233, 1983.

Kennel, C. F., and H. E. Petschek, Limit on Stably Trapped Particle Fluxes, *J. Geophys. Res.,* , *71*, 1–+, 1966.

Kivelson, M., and D. Southwood, Dynamical consequences of two modes of centrifugal instability in jupiter's outer magnetosphere, *Journal of Geophysical Research: Space Physics*, *110*(A12), 2005.

Kolmašová, I., M. Imai, O. Santolík, W. S. Kurth, G. B. Hospodarsky, D. A. Gurnett, J. E. Connerney, and S. J. Bolton, Discovery of rapid whistlers close to jupiter implying lightning rates similar to those on earth, *Nature Astronomy*, *2*(7), 544–548, 2018.

Krupp, N., A. Lagg, S. Livi, B. Wilken, J. Woch, E. Roelof, and D. Williams, Global flows of energetic ions in jupiter's equatorial plane: First-order approximation, *Journal of Geophysical Research: Space Physics*, *106*(A11), 26,017–26,032, 2001.

Kurth, W., G. Hospodarsky, D. Kirchner, B. Mokrzycki, T. Averkamp, W. Robison, C. Piker, M. Sampl, and P. Zarka, The juno waves investigation, *Space Science Reviews*, *213*, 347–392, 2017.

Kurth, W. S., et al., Juno plasma wave observations at ganymede, *Geophysical research letters*, *49*(23), e2022GL098,591, 2022.

Lauben, D. S., U. S. Inan, T. F. Bell, and D. Gurnett, Source characteristics of elf/vlf chorus, *Journal of Geophysical Research: Space Physics*, *107*(A12), SMP–10, 2002.

Li, W., Q. Ma, R. Thorne, J. Bortnik, C. Kletzing, W. Kurth, G. Hospodarsky, and Y. Nishimura, Statistical properties of plasmaspheric hiss derived from van allen probes data and their effects on radiation belt electron dynamics, *Journal of Geophysical Research: Space Physics*, *120*(5), 3393–3405, 2015.

Li, W., X.-C. Shen, J. Menietti, Q. Ma, X.-J. Zhang, W. Kurth, and G. Hospodarsky, Global distribution of whistler mode waves in jovian inner magnetosphere, *Geophysical Research Letters*, *47*(15), e2020GL088,198, 2020.

Li, W., et al., Themis analysis of observed equatorial electron distributions responsible for the chorus excitation, *Journal of Geophysical Research: Space Physics*, *115*(A6), 2010.

Li, W., et al., Driver of energetic electron precipitation in the vicinity of ganymede, *Geophysical Research Letters*, *50*(6), e2022GL101,555, 2023.

Ma, Q., et al., Energetic electron distributions near the magnetic equator in the jovian plasma sheet and outer radiation belt using juno observations, *Geophysical Research Letters*, *48*(24), e2021GL095,833, 2021.

Mauk, B., and N. Fox, Electron radiation belts of the solar system, *Journal of Geophysical Research: Space Physics*, *115*(A12), 2010.

Mauk, B., D. Mitchell, R. McEntire, C. Paranicas, E. Roelof, D. Williams, S. Krimigis, and A. Lagg, Energetic ion characteristics and neutral gas interactions in jupiter's magnetosphere, *Journal of Geophysical Research: Space Physics*, *109*(A9), 2004.

Mauk, B., et al., The jupiter energetic particle detector instrument (jedi) investigation for the juno mission, *Space Science Reviews*, *213*, 289–346, 2017.

Mauk, B. H., and J. Saur, Equatorial electron beams and auroral structuring at jupiter, *Journal of Geophysical Research: Space Physics*, *112*(A10), 2007.

Menietti, J., Y. Shprits, R. Horne, E. Woodfield, G. Hospodarsky, and D. Gurnett, Chorus, ech, and z mode emissions observed at jupiter and saturn and possible electron acceleration, *Journal of Geophysical Research: Space Physics*, *117*(A12), 2012.

Menietti, J., T. Averkamp, M. Imai, W. Kurth, G. Clark, F. Allegrini, J. Groene, J. Faden, and S. Bolton, Low-latitude whistler-mode and higher-latitude z-mode emission at jupiter observed by juno, *Journal of Geophysical Research: Space Physics*, *126*(2), e2020JA028,742, 2021a.

Menietti, J., T. Averkamp, W. Kurth, J. Faden, and S. Bolton, Survey and analysis of whistler- and z-mode emission in the juno extended mission, *Journal of Geophysical Research: Space*

Physics, *128*(12), e2023JA032,037, 2023a.

Menietti, J., P. Yoon, T. Averkamp, W. Kurth, J. Faden, F. Allegrini, P. Kollmann, and S. Bolton, Wave and particle analysis of z-mode and o-mode emission in the jovian inner magnetosphere, *Journal of Geophysical Research: Space Physics*, p. e2022JA031199, 2023b.

Menietti, J., et al., Analysis of whistler-mode and z-mode emission in the juno primary mission, *Journal of Geophysical Research: Space Physics*, *126*(11), e2021JA029,885, 2021b.

Meredith, N. P., R. B. Horne, A. Sicard-Piet, D. Boscher, K. H. Yearby, W. Li, and R. M. Thorne, Global model of lower band and upper band chorus from multiple satellite observations, *Journal of Geophysical Research: Space Physics*, *117*(A10), 2012.

Murakami, G., et al., Response of jupiter's inner magnetosphere to the solar wind derived from extreme ultraviolet monitoring of the io plasma torus, *Geophysical Research Letters*, *43*(24), 12–308, 2016.

Nénon, Q., A. Sicard, and S. Bourdarie, A new physical model of the electron radiation belts of jupiter inside europa's orbit, *Journal of Geophysical Research: Space Physics*, *122*(5), 5148–5167, 2017.

Palmaerts, B., M. F. Vogt, N. Krupp, D. Grodent, and B. Bonfond, Dawn-dusk asymmetries in jupiter's magnetosphere, *Dawn-dusk asymmetries in planetary plasma environments*, pp. 307–322, 2017.

Roussos, E., P. Kollmann, N. Krupp, C. Paranicas, K. Dialynas, N. Sergis, D. Mitchell, D. Hamilton, and S. Krimigis, Drift-resonant, relativistic electron acceleration at the outer planets: Insights from the response of saturn's radiation belts to magnetospheric storms, *Icarus*, *305*, 160–173, 2018.

Saur, J., et al., Wave-particle interaction of alfvén waves in jupiter's magnetosphere: Auroral and magnetospheric particle acceleration, *Journal of Geophysical Research: Space Physics*, *123*(11), 9560–9573, 2018.

Sazhin, S., K. Bullough, and M. Hayakawa, Auroral hiss: A review, *Planetary and space science*, *41*(2), 153–166, 1993.

Schneider, N. M., and J. T. Trauger, The structure of the io torus, *The Astrophysical Journal*, *450*, 450, 1995.

Shprits, Y., J. Menietti, X. Gu, K.-C. Kim, and R. Horne, Gyroresonant interactions between the radiation belt electrons and whistler mode chorus waves in the radiation environments of earth, jupiter, and saturn: A comparative study, *Journal of Geophysical Research: Space Physics*, *117*(A11), 2012.

Shprits, Y. Y., et al., Strong whistler mode waves observed in the vicinity of jupiter's moons, *Nature communications*, *9*(1), 3131, 2018.

Teng, S., X. Tao, and W. Li, Typical characteristics of whistler mode waves categorized by their spectral properties using van allen probes observations, *Geophysical Research Letters*, *46*(7), 3607–3614, 2019.

Tomás, A. T., J. Woch, N. Krupp, A. Lagg, K.-H. Glassmeier, and W. S. Kurth, Energetic electrons in the inner part of the jovian magnetosphere and their relation to auroral emissions, *Journal of Geophysical Research: Space Physics*, *109*(A6), 2004.

Tsurutani, B. T., and E. J. Smith, Postmidnight chorus: A substorm phenomenon, *Journal of Geophysical Research*, *79*(1), 118–127, 1974.

Tsurutani, B. T., and E. J. Smith, Two types of magnetospheric elf chorus and their substorm dependences, *Journal of Geophysical Research*, *82*(32), 5112–5128, 1977.

Vogt, M. F., M. G. Kivelson, K. K. Khurana, R. J. Walker, M. Ashour-Abdalla, and E. J. Bunce, Simulating the effect of centrifugal forces in jupiter's magnetosphere, *Journal of Geophysical Research: Space Physics*, *119*(3), 1925–1950, 2014.

Waldrop, L., E. Roelof, and T. Fritz, Three-dimensional convective flows of energetic ions in jupiter's equatorial magnetosphere, *Journal of Geophysical Research: Space Physics*, *120*(12), 10–506, 2015.

Wang, D., Y. Y. Shprits, I. S. Zhelavskaya, O. V. Agapitov, A. Y. Drozdov, and N. A. Aseev, Analytical chorus wave model derived from van allen probe observations, *Journal of Geophysical Research: Space Physics*, *124*(2), 1063–1084, 2019.

Wang, J.-z., J.-n. Ma, Z.-x. Huo, Y. Xiong, and D. Tian, Statistical study of energetic electrons in jupiter's inner magnetosphere by juno/jedi, *Advances in Space Research*, *67*(5), 1709–1720, 2021.

Woodfield, E. E., R. B. Horne, S. A. Glauert, J. D. Menietti, and Y. Shprits, The origin of jupiter's outer radiation belt, *Journal of Geophysical Research: Space Physics*, *119*(5), 3490–3502, 2014.

Yuan, C., Y. Zuo, E. Roussos, Y. Wei, Y. Hao, Y. Sun, and N. Krupp, Large-scale episodic enhancements of relativistic electron intensities in jupiter's radiation belt, *Earth and Planetary Physics*, *5*(4), 314–326, 2021.

Yuan, C., E. Roussos, Y. Wei, N. Krupp, Z. Liu, and J. Wang, Galileo observation of electron spectra dawn-dusk asymmetry in the middle jovian magnetosphere: Evidence for convection electric field, *Geophysical Research Letters*, *51*(1), e2023GL105,503, 2024.

Zhao, H., et al., Plasmaspheric hiss waves generate a reversed energy spectrum of radiation belt electrons, *Nature Physics*, *15*(4), 367–372, 2019.